# Giant spectral transformations in plasmon-enhanced difference-frequency generation with polychromatic light



2016 J. Opt. 18 125503

(http://iopscience.iop.org/2040-8986/18/12/125503)

OPEN ACCESS
IOP Publishing
Journal of Optics
J. Opt. **18** (2016) 125503 (8pp)
doi:10.1088/2040-8978/18/12/125503

# Giant spectral transformations in plasmon-enhanced difference-frequency generation with polychromatic light

**Franklin Che, Sergey A Ponomarenko and Michael Cada**

Department of Electrical and Computer Engineering, Dalhousie University, Halifax, NS, B3H 4R2 Canada

E-mail: franklin.che@dal.ca

Received 28 July 2016, revised 26 September 2016
Accepted for publication 7 October 2016
Published 15 November 2016

**Abstract**

We theoretically study the generation of mid-infrared light through difference-frequency excitation using a single dual-wavelength coherent femtosecond laser source. The difference-frequency wave is generated from the surface of a thin gold film in the Kretschmann coupling geometry due to the surface nonlinearity of the film. We show a clear enhancement of the difference-frequency wave around the surface plasmon polariton coupling angle of the incident fundamental wave. We also show an enormous shift and modification of the difference-frequency spectrum near surface plasmon resonance. We discuss the discovered spectral change dependence on the source pulse duration and incidence angle of the fundamental wave. Our findings have an enormous potential for use in difference-frequency surface sensing and spectroscopy applications.

Keywords: difference-frequency generation, surface plasmons, nonlinear optics, spectra

(Some figures may appear in colour only in the online journal)

## 1. Introduction

Although the study of nonlinear frequency conversion in metals goes back to the beginning of nonlinear optics [1–7], there has been renewed interest in this field recently. This new interest is due to the recent growth in the field of plasmonics, which studies the localization and enhancement of electromagnetic fields through the collective oscillation of conduction electrons in metals. The combination of nonlinearity and plasmonic effects has opened up a whole new area of fundamental research where the generation, modification and enhancement of harmonic frequencies can be studied under a variety of conditions and circumstances [8–13].

Nonlinear studies of surface plasmon excitations in metals are focused primarily on quadratic nonlinearities such as second-harmonic generation (SHG), sum-frequency generation (SFG) and difference-frequency generation (DFG). This is due to the simplicity of these processes and the ability to discriminate the bulk response from the surface response using the inversion symmetry of most metals [13–15]. These quadratic plasmonic nonlinear processes have led to applications in sensing, spectroscopy and the development of new coherent light sources [16–21]. Most nonlinear plasmonic applications, such as infrared-visible nonlinear spectroscopy [22], are based on quasi-monochromatic light sources, where two distinct monochromatic sources are needed for both SFG [23] and DFG [24] spectroscopy. DFG in particular has also been shown to be the most widely used method to generate mid-infrared (MIR) ultra short pulses [25–29], which are very useful as a source for sensing many important organic and inorganic molecules. This is because these molecules have strong absorption peaks within this spectral range [30] and the fact that the DFG process is very sensitive to changes in the surfaces being studied at the molecular level [31, 32].

We propose using a highly collimated polychromatic source to generate a difference-frequency wave (DFW) in the mid-infrared through reflection from a thin metal film

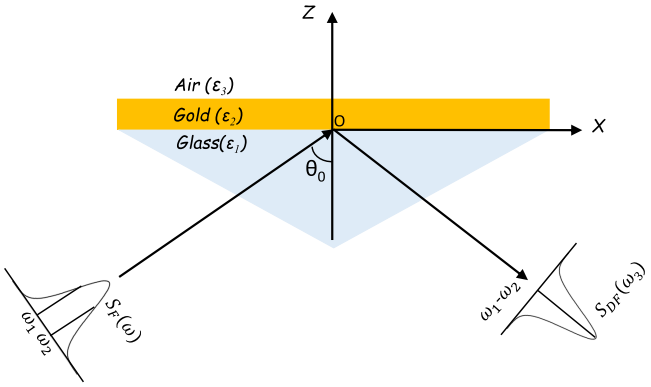


**Figure 1.** Illustration of the Kretschmann configuration.

arranged in the Kretschmann configuration close to the surface plasmon coupling angle. The generation of MIR sources using DFG usually involves frequency mixing of two monochromatic laser sources [25–29]. We are, however, using a single polychromatic source, which eliminates the need for multiple sources and also has the added advantage of generating spectral signatures and enhancing the DFW close to the plasmon resonance angle. The spectral signatures of a surface sum-frequency wave reflected from a thin gold film using polychromatic light have been previously reported [33], with significant spectral shifts in the spectrum shown close to plasmon resonance. We report more pronounced shifts and enhancement in the difference-frequency spectrum close to plasmon resonance.

## 2. Theory

We use the Kretschmann configuration to illuminate the gold thin film as shown in figure 1. The gold film is deposited on a glass substrate ($\epsilon_1 = 2.25$) and has a thickness $d$ and a relative permittivity $\epsilon_2(\omega)$. The permittivity of the dielectric above the thin film is $\epsilon_3$ and the source plane is assumed to be at the origin.

The light source is assumed to generate a highly collimated and fully spatially coherent plane wave [34–36]. The incident fundamental wave (FW) with a spectral amplitude $A(\omega)$ is represented by

$$\mathbf{E}_0(x, z, \omega, \theta_0) = A(\omega)\left(\frac{k_{1z}}{k_1}\mathbf{e}_x - \frac{k_x}{k_1}\mathbf{e}_z\right)e^{\mathrm{i}(k_x x + k_{1z} z)}, \quad (1)$$

where $\mathbf{k}_1 = (k_x, 0, k_{1z})$ and $k_1 = (\omega/c)\sqrt{\varepsilon_1}$, with $\mathbf{k}_1$ expressed in terms of the incident angle $\theta_0$ as $k_x = k_1 \sin\theta_0$ and $k_{1z} = k_1 \cos\theta_0$. The energy spectrum of the incident pulse can be written as [37]

$$S_0(\omega) \propto |\mathbf{E}_0(x, z, \omega, \theta_0)|^2. \quad (2)$$

Whenever the FW is incident on the metal, it undergoes multiple reflections in the thin film and the total reflected FW from the film can be calculated using the Airy summation [38] and is given by

$$\mathbf{E}_r(x, z, \omega, \theta_0) = A(\omega)\left(-\frac{k_{1z}}{k_1}\mathbf{e}_x - \frac{k_x}{k_1}\mathbf{e}_z\right) \times \tilde{r}_{12}(\omega, \theta_0)e^{\mathrm{i}(k_x x - k_{1z} z)}, \quad (3)$$

where $\tilde{r}_{12}(\omega, \theta_0)$ is the Fresnel reflection coefficient for p-polarization given by [39]

$$\tilde{r}_{12}(\omega, \theta_0) = \frac{r_{12} + r_{23}e^{\mathrm{i}2k_{2z}d}}{1 + r_{12}r_{23}e^{\mathrm{i}2k_{2z}d}}, \quad (4)$$

with $k_{2z} = \sqrt{k_2^2 - k_x^2}$, $k_2 = (\omega/c)\sqrt{\varepsilon_2}$ and $r_{\alpha\beta}$ represents the reflection coefficient of the interface between media $\alpha$ and $\beta$, ($\alpha, \beta = 1, 2, 3$). From equation (3), the reflected energy spectrum can be written as

$$S_r(\omega, \theta_0) \propto |\mathbf{E}_r(x, z, \omega, \theta_0)|^2. \quad (5)$$

The incident wave excites surface polarizations at both the lower and upper interfaces of the gold film. The general $i^{th}$ component of the difference-frequency polarization field is given by [40]

$$P_i(\mathbf{r}, \omega_3) = \varepsilon_0 \sum_{jk}\int_{-\infty}^{\infty}\frac{\mathrm{d}\omega_1}{2\pi}\chi^{(2)}_{S,ijk}(\omega_3; \omega_1, \omega_2) \times E_j(\mathbf{r}, \omega_1)E_k^*(\mathbf{r}, \omega_2), \quad (6)$$

where ($i, j, k = x, y, z$), $\omega_1$ and $\omega_2$ are the pump frequencies within the incident fundamental pulse bandwidth, $\omega_3 = \omega_1 - \omega_2$ represents the generated difference frequency and the asterisk (*) denotes the complex conjugate. $\chi^{(2)}_{S,ijk}(\omega_3; \omega_1, \omega_2)$ is the nonlinear surface susceptibility tensor of the DFG process. For p-polarized light, the relevant non-trivial contributions to the surface DFG susceptibility are $\chi^{(2)}_{S,zzz}(\omega_3; \omega_1, \omega_2)$, $\chi^{(2)}_{S,xxz}(\omega_3; \omega_1, \omega_2)$ and $\chi^{(2)}_{S,xzx}(\omega_3; \omega_1, \omega_2)$ [41].

We use equation (6) to evaluate the polarization at the lower ($\mathbf{P}^{<}_{x,z}$) and upper ($\mathbf{P}^{>}_{x,z}$) interfaces of the thin film as we show in the appendix. These lower and upper interface polarizations act as source currents at the difference frequency, and the resulting DFW is given by

$$E_i(\mathbf{r}, \omega) = \frac{(\omega/c)^2}{\varepsilon_0}\sum_j\int \mathrm{d}\mathbf{r}' G_{ij}(\mathbf{r}, \mathbf{r}', \omega)P_j(\mathbf{r}', \omega). \quad (7)$$

$G_{ij}(\mathbf{r}, \mathbf{r}')$ is the dyadic Green's function given by [15]

$$G_{ij}(\mathbf{r}, \mathbf{r}') = \left[\delta_{ij} + \frac{1}{k^2}\nabla_i\nabla_j\right]G_0(\mathbf{r}, \mathbf{r}', \omega), \quad (8)$$

where $G_0$ is the scalar Green's function and can be expanded using Weyl's identity [34] to obtain

$$G_0(\mathbf{r}, \mathbf{r}', \omega) = \frac{\mathrm{e}^{\mathrm{i}k|\mathbf{r}-\mathbf{r}'|}}{4\pi|\mathbf{r} - \mathbf{r}'|} = \frac{\mathrm{i}}{8\pi^2}\int_{-\infty}^{\infty}\frac{\mathrm{d}k_x}{k_z}\mathrm{e}^{\mathrm{i}k_x(x-x') + \mathrm{i}k_z|z-z'|}, \quad (9)$$

where $k_x$ and $k_z$ represent the longitudinal and transverse components of the propagation vector.

The contribution to the DFW radiated into the lower half-space from the nonlinear polarization at the lower metal interface is obtained by substituting $P^{<}_{x,z}$ into equation (7), yielding

$$\mathbf{E}^{<}_{x,\mathrm{bottom}}(x,\, z,\, \omega_3,\, \theta_0) = \frac{\mathrm{i}\omega_3}{4\pi\sqrt{\varepsilon_0\varepsilon_1}}(P^{<}_{0x}\cos\theta_0 - P^{<}_{0z}\sin\theta_0) \times e^{\mathrm{i}(k_x(\omega_3)x - k_{1z}(\omega_3)z)}\mathbf{e}_x, \tag{10}$$

where all quantities are evaluated at the difference frequency $\omega_3$, with $\mathbf{k}_1(\omega_3) = (k_x(\omega_3),\, 0,\, k_{1z}(\omega_3))$ and $\mathbf{k}_2(\omega_3) = (k_x(\omega_3),\, 0,\, k_{2z}(\omega_3))$.

$P^{<}_{x,z}$ contributes further to the DFW when the field above (equation (10)) is partially transmitted through the metal film and reflected from the top metal boundary back into the lower half-space as

$$\mathbf{E}^{<}_{x,\mathrm{top}}(x,\, z,\, \omega_3,\, \theta_0) = \frac{\mathrm{i}\omega_3}{4\pi\sqrt{\varepsilon_0\varepsilon_1}}(P^{<}_{0x}\cos\theta_0 - P^{<}_{0z}\sin\theta_0) \times \mathrm{e}^{\mathrm{i}(k_x(\omega_3)x - k_{1z}(\omega_3)z)}\frac{r_{23}t_{12}\mathrm{e}^{\mathrm{i}2k_{2z}(\omega_3)d}}{1 + r_{12}r_{23}\mathrm{e}^{\mathrm{i}2k_{2z}(\omega_3)d}}\mathbf{e}_x. \tag{11}$$

$t_{\alpha\beta}$ is the transmission coefficient of the interface between media $\alpha$ and $\beta$, ($\alpha$, $\beta = 1, 2, 3$). The corresponding z-component of the radiated DFW due to the polarization at the bottom interface of the film is given by

$$\mathbf{E}^{<}_{z,\mathrm{bottom}}(x,\, z,\, \omega_3,\, \theta_0) = \frac{\mathrm{i}\omega_3}{4\pi\sqrt{\varepsilon_0\varepsilon_1}}(P^{<}_{0z}\sin\theta_0\tan\theta_0 - P^{<}_{0x}\sin\theta_0) \times \mathrm{e}^{\mathrm{i}(k_x(\omega_3)x - k_{1z}(\omega_3)z)}\mathbf{e}_z, \tag{12}$$

and after undergoing reflection from the upper interface, it becomes

$$\mathbf{E}^{<}_{z,\mathrm{top}}(x,\, z,\, \omega_3,\, \theta_0) = \frac{\mathrm{i}\omega_3}{4\pi\sqrt{\varepsilon_0\varepsilon_1}}(P^{<}_{0z}\sin\theta_0\tan\theta_0 - P^{<}_{0x}\sin\theta_0) \times \mathrm{e}^{\mathrm{i}(k_x(\omega_3)x - k_{1z}(\omega_3)z)}\frac{r_{23}t_{12}\mathrm{e}^{\mathrm{i}2k_{2z}(\omega_3)d}}{1 + r_{12}r_{23}\mathrm{e}^{\mathrm{i}2k_{2z}(\omega_3)d}}\mathbf{e}_z. \tag{13}$$

The contribution to the difference-frequency field from the polarization $P^{>}_{x,z}$ at the upper metal interface which is radiated into the lower half-space is given by

$$\mathbf{E}^{>}_{x,\mathrm{top}}(x,\, z,\, \omega_3,\, \theta_0) = \frac{\mathrm{i}\omega_3}{4\pi\sqrt{\varepsilon_0\varepsilon_2(\omega_3)}}(P^{>}_{0x}\cos\theta_0 - P^{>}_{0z}\sin\theta_0) \times \mathrm{e}^{\mathrm{i}(k_x(\omega_3)x - k_{1z}(\omega_3)z)}\frac{t_{12}\mathrm{e}^{\mathrm{i}2k_{2z}(\omega_3)d}}{1 + r_{12}r_{23}\mathrm{e}^{\mathrm{i}2k_{2z}(\omega_3)d}}\mathbf{e}_x, \tag{14}$$

and

$$\mathbf{E}^{>}_{z,\mathrm{top}}(x,\, z,\, \omega_3,\, \theta_0) = \frac{\mathrm{i}\omega_3}{4\pi\sqrt{\varepsilon_0\varepsilon_2(\omega_3)}} \times (P^{>}_{0z}\sin\theta_0\tan\theta_0 - P^{>}_{0x}\sin\theta_0) \times \mathrm{e}^{\mathrm{i}(k_x(\omega_3)x - k_{1z}(\omega_3)z)}\frac{t_{12}\mathrm{e}^{\mathrm{i}2k_{2z}(\omega_3)d}}{1 + r_{12}r_{23}\mathrm{e}^{\mathrm{i}2k_{2z}(\omega_3)d}}\mathbf{e}_z, \tag{15}$$

where all quantities are evaluated at the difference frequency $\omega_3$.

From equations (10)–(15), the components of the DFW can be written as

$$\mathbf{E}_x(x,\, z,\, \omega_3,\, \theta_0) = \mathbf{E}^{<}_{x,\mathrm{bottom}}(x,\, z,\, \omega_3,\, \theta_0) + \mathbf{E}^{<}_{x,\mathrm{top}}(x,\, z,\, \omega_3,\, \theta_0) + \mathbf{E}^{>}_{x,\mathrm{top}}(x,\, z,\, \omega_3,\, \theta_0), \tag{16}$$

and

$$\mathbf{E}_z(x,\, z,\, \omega_3,\, \theta_0) = \mathbf{E}^{<}_{z,\mathrm{bottom}}(x,\, z,\, \omega_3,\, \theta_0) + \mathbf{E}^{<}_{z,\mathrm{top}}(x,\, z,\, \omega_3,\, \theta_0) + \mathbf{E}^{>}_{z,\mathrm{top}}(x,\, z,\, \omega_3,\, \theta_0). \tag{17}$$

The energy spectrum of the DFW can then be conveniently written as

$$\mathbf{S}(\omega_3,\, \theta_0) \propto |E_x(x,\, z,\, \omega_3,\, \theta_0)\mathbf{e}_x + E_z(x,\, z,\, \omega_3,\, \theta_0)\mathbf{e}_z|^2. \tag{18}$$

## 3. Results

We use a dual-wavelength self-mode-locked Ti:sapphire laser [42], with a pulse duration ($t_p$) of 50 fs and peaks at $\lambda = 853$ nm ($\omega = 2.208 \times 10^{15}$ rads s$^{-1}$) and $\lambda = 767$ nm ($\omega = 2.456 \times 10^{15}$ rads s$^{-1}$) with the normalized spectral amplitude $A(\omega)$ shown in figure 2(a). The pulse duration defines the bandwidth of the input gaussian pulse $\left(\Delta\omega \approx \frac{0.44}{t_p}\right)$. When this FW is incident on the 50 nm gold thin film, the reflected FW is evaluated using equation (5), with the dielectric permittivity of the gold film evaluated by interpolating the experimental values of Johnson and Christy [43]. This reflected field is shown in figure 2(b).

The holes in the reflected FW spectrum are due to the coupling of the incident wave to surface plasmon polaritons (SPP). The SPP coupling angle for $\epsilon_3 = 1$(air) is given by [15, 33]

$$\theta_c(\omega) = \arcsin\left[\sqrt{\frac{\varepsilon_2(\omega)}{\varepsilon_1(\varepsilon_2(\omega) + 1)}}\right]. \tag{19}$$

For $\lambda = 767$ nm and $\lambda = 853$ nm, the corresponding SPP coupling angles, calculated from equation (19), are 43.3° and 42.8° respectively, which coincide well with the plasmon resonance angles in figure 2(b).

To evaluate the DFW, we use the hydrodynamic model of the difference-frequency surface susceptibility developed in [44]. The nonvanishing susceptibility components are

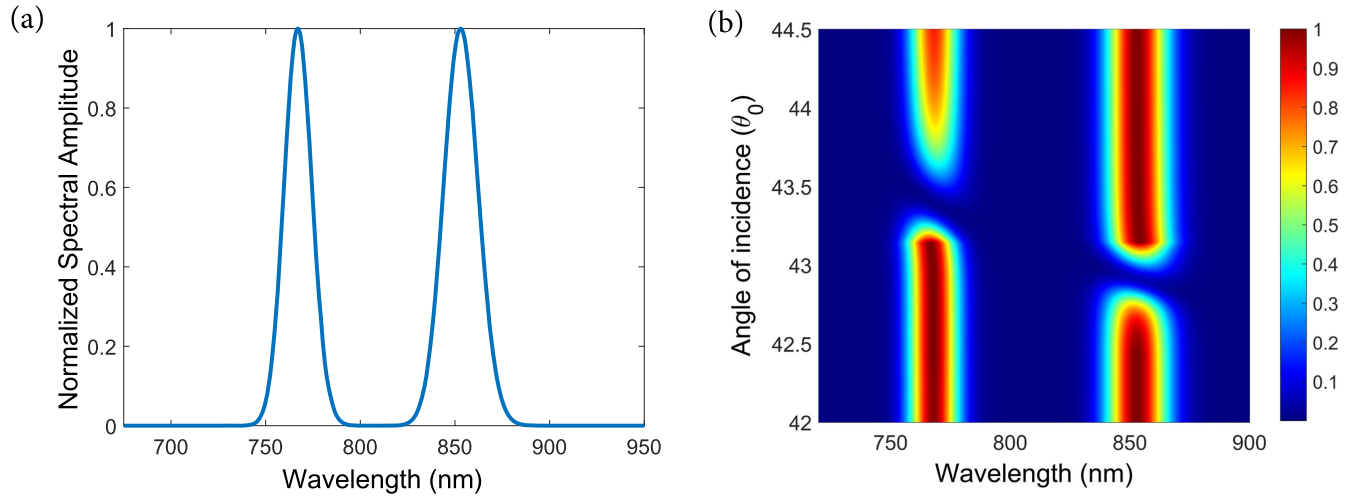


**Figure 2.** Far-field spectra of ($a$) incident fundamental wave and ($b$) the reflected fundamental spectrum from metal film. Incident pulse duration is $t_p = 50$ fs.

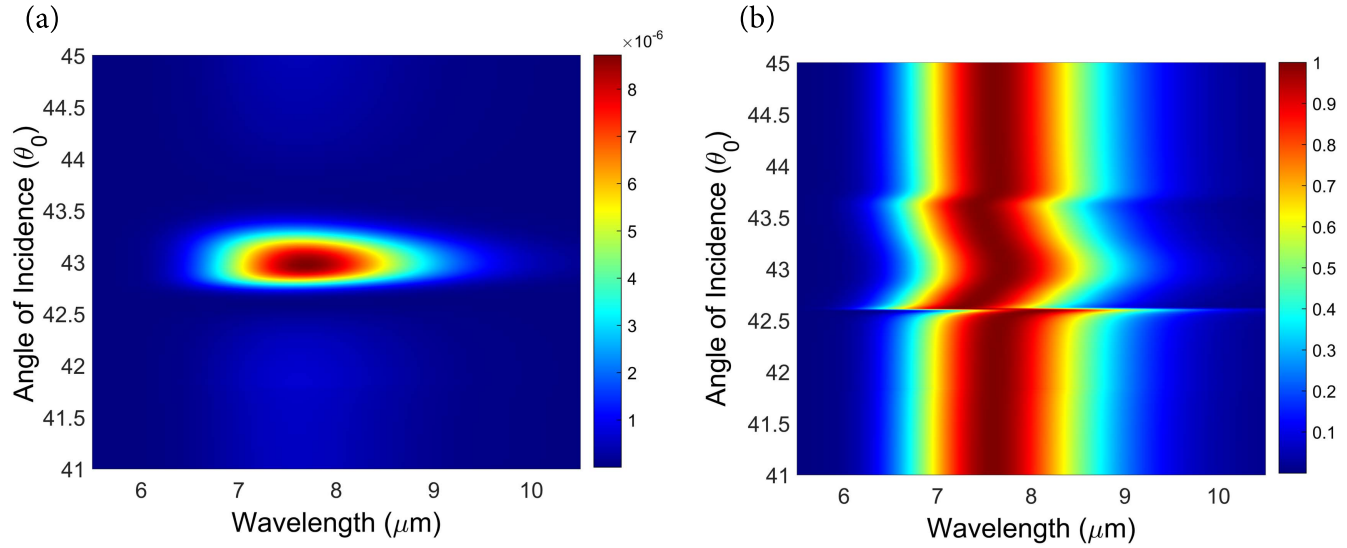


**Figure 3.** Reflected far-field spectra of ($a$) DFW and ($b$) normalized DFW. Incident pulse duration is $t_p = 50$ fs.

given by

$$\chi^{(2)}_{S,zzz}(\omega_3;\,\omega_1,\,\omega_2) = -\frac{a(\omega_1,\,\omega_2)[\varepsilon_2(\omega_1)-1][\varepsilon_2^*(\omega_2)-1]}{64\pi^2\varepsilon_2(\omega_1)\varepsilon_2^*(\omega_2)n_B e},$$

$$\chi^{(2)}_{S,xzx}(\omega_3;\,\omega_1,\,\omega_2) = -\frac{2b(\omega_1,\,\omega_2)[\varepsilon_2(\omega_1)-1][\varepsilon_2^*(\omega_2)-1]\omega_2}{64\pi^2\omega_3\varepsilon_2(\omega_1)n_B e},$$

$$\chi^{(2)}_{S,xxz}(\omega_3;\,\omega_1,\,\omega_2) = -\frac{2b(\omega_1,\,\omega_2)[\varepsilon_2(\omega_1)-1][\varepsilon_2^*(\omega_2)-1]\omega_1}{64\pi^2\omega_3\varepsilon_2^*(\omega_2)n_B e}, \quad (20)$$

where $n_B$ is the equilibrium free-electron density in the bulk. The dimensionless parameters $a(\omega_1, \omega_2)$ and $b(\omega_1, \omega_2)$ are frequency independent when $\omega_1$ and $\omega_2$ are well below the plasma frequency $\omega_p$, which is true in our case $\left(\frac{\omega_{1,2}}{\omega_p} \approx 0.15\right)$. We use $b(\omega_1, \omega_2) = -1$ and $a(\omega_1, \omega_2) = -12.9$ [41]. To evaluate the DFW we use equation (18).

Figure 3(a) shows the reflected DFW energy spectrum for a 50 fs FW. The DFW peak is centered around 7.70 $\mu$m, which corresponds to the frequency difference ($\omega_3$) of the peaks in our fundamental wave, with $\omega_3 = \omega_1 - \omega_2$, where ($\omega_1 = 2.456 \times 10^{15}$ rads s$^{-1}$) , and ($\omega_2 = 2.208 \times 10^{15}$rads s$^{-1}$). Figure 3(a) also shows an enhancement of the DFW around the plasmon resonance angles of both peaks in the FW, which is between 42.6° and 43.5°, with a maximum enhancement of 14 times the off-resonance spectral amplitude. The enhancement of the DFW is clearly due to the coupling of the FW to surface plasmon polaritons, which has also been reported before in the Kretschmann configuration for SHG [13] and SFG [33].

We can better highlight the spectral effects of DFG in our system by normalizing the DFW spectrum to the corresponding maximum for each angle of incidence [33] as shown

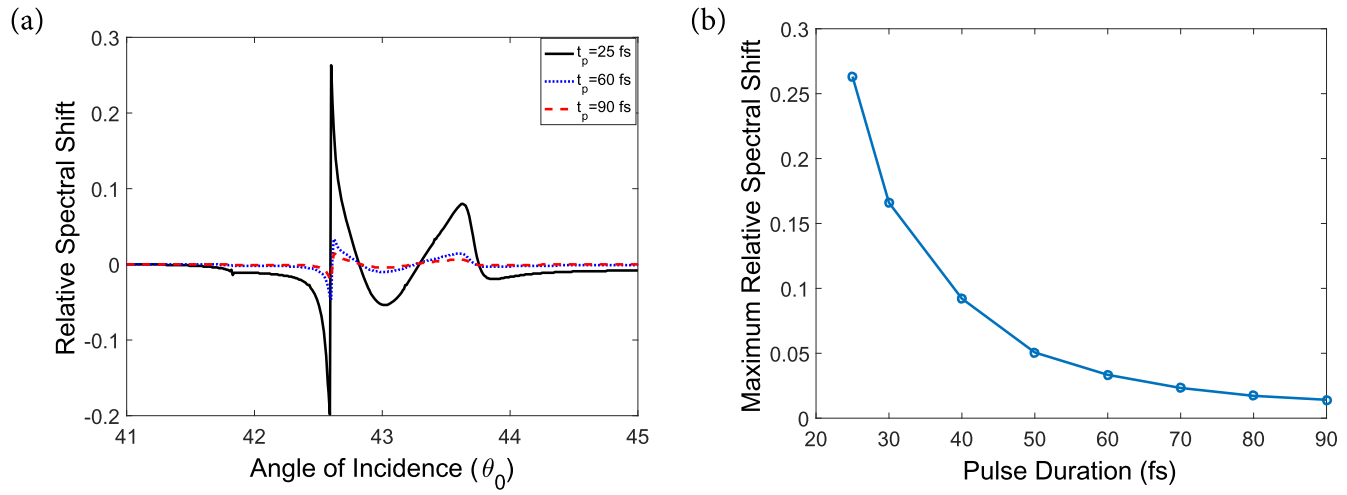


**Figure 4.** (*a*) Dependence of relative spectral shifts on pulse duration and angle of incidence. (*b*) Maximum spectral shift as a function of pulse duration.

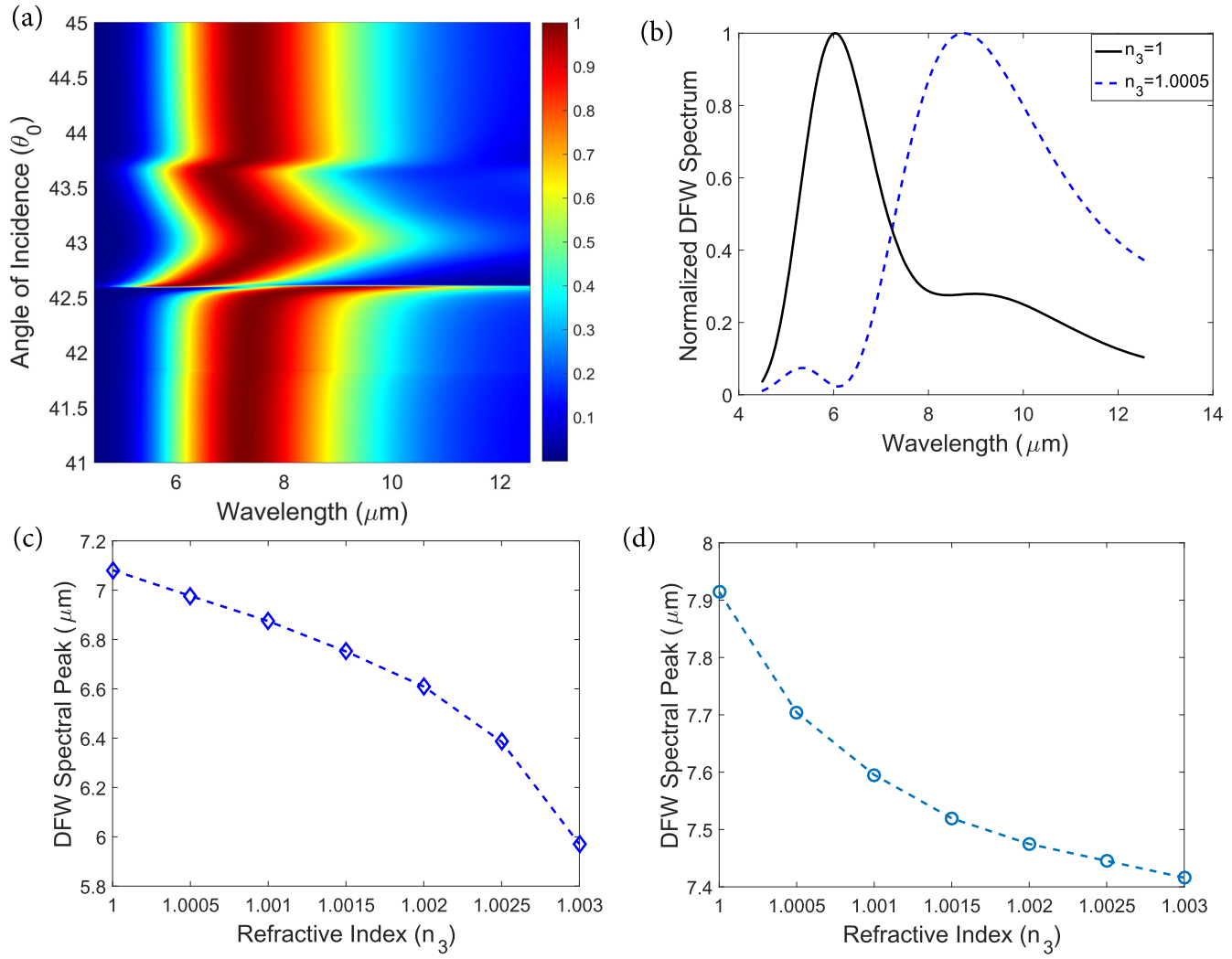


**Figure 5.** (*a*) Normalized far-field spectra of DFW with a source pulse duration of $t_p = 25$ fs. (*b*) Normalized DFW spectral shift close to plasmon resonance at $\theta_0 = 42.6°$ for $\Delta n_3 = 5 \times 10^{-4}$ . (*c*) DFW peak dependence on refractive index $n_3$ at $\theta_0 = 42.8°$. (*d*) DFW peak dependence on refractive index $n_3$ at $\theta_0 = 42.5°$.

in figure 3(b). We observe significant shifts in our spectrum between the plasmon resonance angles of 42.6° and 43.5°. This shift is more pronounced at the lower edge of the plasmon resonance angular range around 42.6°. To explore the dependence of these spectral shifts on the pulse duration or angle of incidence, we determine the so-called relative spectral shift $\left(\frac{\Delta\lambda}{\lambda_0}\right)$ [33], where $\lambda_0 = 7.70\ \mu$m. This dependence is shown in figure 4(a), where we notice a clear increase in the spectral shift with decreasing pulse duration. Figure 4(b) illustrates this dependency better, showing the maximum spectral shift for pulse durations ranging from 25 fs to 90 fs. A fundamental wave with a short pulse duration has a large bandwidth. This means a wider range of frequencies are coupled into surface plasmons and with each frequency having a slightly different plasmonic and nonlinear response, the total effect on the DFW spectrum is more pronounced.

To further examine the spectrum of the DFW, we display the normalized DFW spectra for a 25 fs FW as shown in figure 5(a), with the maximum spectral shift seen around $\theta_0 = 42.6°$. Figure 5(b) shows a colossal spectral shift for a small change in the refractive index of the dielectric material ($n_3$) with $\Delta n_3 = 5 \times 10^{-4}$, at the angle of incidence corresponding to the maximum shift in figure 5(a). We also observe significant spectral shifts varying $n_3$ above and below the maximum angle, as shown in figures 5(c) and (d) respectively. Linear and nonlinear spectral shifts close to resonance are both based on the frequency dependence of the plasmonic response of metal thin films, which have frequency-dependent permittivities and nonlinear susceptibilities. The DFW spectral shifts are more pronounced compared to those engendered by a linear 7.70 $\mu$m femtosecond pulse coupled into surface plasmon polaritons in the Kretschmann configuration because of the nonlinear interaction of the plasmon-enhanced FW which generates the DFW. Such sensitivity to small changes in refractive index could be very useful for surface sensing applications.

Besides the spectral shifts, we also observe changes in the shape of the DFW spectrum close to resonance. We can clearly observe the evolution of the shape of the DFW when we vary the angle of incidence slightly from $\theta_0 = 42.60°$ to $\theta_0 = 42.62°$ in figure 6. Such sensitivity of the spectral shape on small angular variations can also be leveraged for sensing applications.

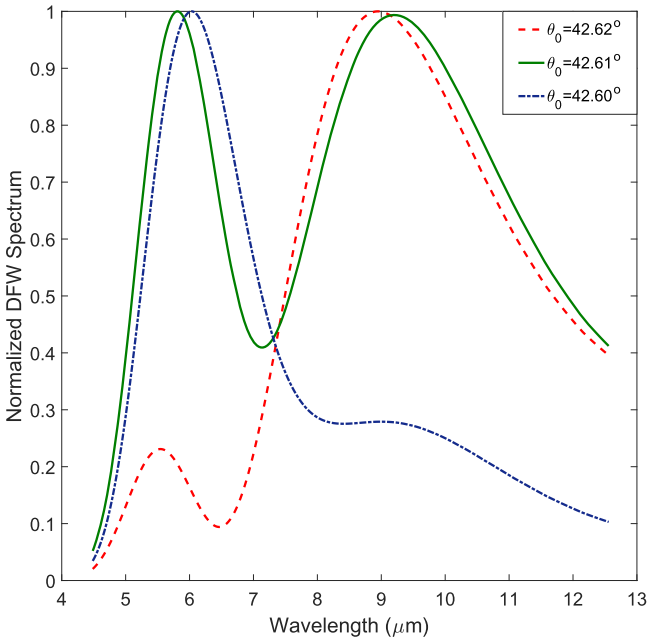


**Figure 6.** Normalized far-field DFW energy spectrum close to resonance showing changes in the spectral shape, $n_3 = 1$ and $t_p = 25$ fs.

## 4. Conclusions

We have investigated, theoretically, the generation of a mid-infrared DFW from a thin gold film in the Kretschmann configuration. We used a single dual-wavelength femtosecond laser as our source and gaps were observed in the spectrum of the reflected fundamental wave, which corresponded to the plasmon resonance angles of the individual peaks. The DFW peak amplitude frequency corresponded to the difference between the peak frequencies in our FW, and was clearly enhanced around the plasmon resonance angle of the fundamental wave. We have also shown very large spectral shifts in the DFW close to the surface plasmon resonance angles and also highlighted their dependence on the pulse duration of the fundamental wave, the angle of incidence and changes in the refractive index of dielectric above the metal film. Lastly, changes in the DFW spectral shape close to resonance were also demonstrated. All these features make our system attractive for use as an MIR source and a sensitive surface sensor.

## Appendix. Polarization calculations

The total FW in the glass is a superposition of the incident and reflected waves in equation (1) and equation (3). This is given by

$$\mathbf{E}_1(x, z, \omega, \theta_0) = \mathbf{E}_0(x, z, \omega, \theta_0) + \mathbf{E}_r(x, z, \omega, \theta_0). \quad \text{(A.1)}$$

The normal component of equation (A.1) can be written as

$$\mathbf{E}_{1z}(x, z, \omega, \theta_0) = -\frac{k_x}{k_1} A(\omega) e^{ik_x x}[e^{ik_z z} + \tilde{r}_{12}(\omega, \theta_0) e^{-ik_{1z} z}]\mathbf{e}_z, \quad \text{(A.2)}$$

while the tangential component is written as,

$$\mathbf{E}_{1x}(x, z, \omega, \theta_0) = \frac{k_{1z}}{k_1} A(\omega) e^{ik_x x} \times [e^{ik_z z} - \tilde{r}_{12}(\omega, \theta_0) e^{-ik_{1z} z}]\mathbf{e}_x. \quad \text{(A.3)}$$

By applying the electromagnetic boundary conditions to both the normal and tangential components of the electric field on both sides of the boundary at $z = 0$, we can write down the components of electric field, $E_2^<$ on the lower interface of the

metal. The normal component of the field is given by

$$\mathbf{E}_{2z}^{<}(x,\, z,\, \omega,\, \theta_0) = -\frac{k_x}{k_1}\frac{\varepsilon_1}{\varepsilon_2}A(\omega)\mathrm{e}^{\mathrm{i}k_x x} \times [1 + \tilde{r}_{12}(\omega,\, \theta_0)]\mathrm{e}_z, \quad (A.4)$$

while the tangential component is given by

$$\mathbf{E}_{2x}^{<}(x,\, z,\, \omega,\, \theta_0) = \frac{k_{1z}}{k_1}A(\omega)\mathrm{e}^{\mathrm{i}k_x x}[1 - \tilde{r}_{12}(\omega,\, \theta_0)]\mathrm{e}_x. \quad (A.5)$$

The normal and tangential components of the field in the gold thin film are superpositions of the fields transmitted into the film and that reflected from the upper interface of the thin film. They are given respectively by

$$\mathbf{E}_{2z}(x,\, z,\, \omega,\, \theta_0) = -\frac{k_x}{k_2}A(\omega)\mathrm{e}^{\mathrm{i}k_x x}\frac{t_{12}}{1 + r_{12}r_{23}\mathrm{e}^{\mathrm{i}2k_{2z}d}} \times [\mathrm{e}^{\mathrm{i}k_{2z}z} + r_{23}\mathrm{e}^{\mathrm{i}2k_{2z}d}\mathrm{e}^{-\mathrm{i}k_{2z}z}]\mathrm{e}_z, \quad (A.6)$$

and

$$\mathbf{E}_{2x}(x,\, z,\, \omega,\, \theta_0) = \frac{k_{2z}}{k_2}A(\omega)\mathrm{e}^{\mathrm{i}k_x x}\frac{t_{12}}{1 + r_{12}r_{23}\mathrm{e}^{\mathrm{i}2k_{2z}d}} \times [\mathrm{e}^{\mathrm{i}k_{2z}z} - r_{23}\mathrm{e}^{\mathrm{i}2k_{2z}d}\mathrm{e}^{-\mathrm{i}k_{2z}z}]\mathrm{e}_x. \quad (A.7)$$

The components of the electric field at the upper interface of the gold film, $E_2^{>}$ at $z = d$ are calculated similarly to yield

$$\mathbf{E}_{2z}^{>}(x,\, z,\, \omega,\, \theta_0) = -\frac{k_x}{k_2}A(\omega)\mathrm{e}^{\mathrm{i}k_x x}R_z(\omega,\, \theta_0)\mathrm{e}_z, \quad (A.8)$$

and

$$\mathbf{E}_{2x}^{>}(x,\, z,\, \omega,\, \theta_0) = -\frac{k_{2z}}{k_2}A(\omega)\mathrm{e}^{\mathrm{i}k_x x}R_x(\omega,\, \theta_0)\mathrm{e}_x, \quad (A.9)$$

where

$$R_z(\omega,\, \theta_0) = \frac{t_{12}(1 + r_{23})\mathrm{e}^{\mathrm{i}2k_z d}}{1 + r_{12}r_{23}\mathrm{e}^{\mathrm{i}2k_{2z}d}},$$
$$R_x(\omega,\, \theta_0) = \frac{t_{12}(1 - r_{23})\mathrm{e}^{\mathrm{i}2k_z d}}{1 + r_{12}r_{23}\mathrm{e}^{\mathrm{i}2k_{2z}d}}. \quad (A.10)$$

The polarization at the lower interface of the thin film, $P_{x,z}^{<}$ can then be determined using the electric field components at the lower interface and equation (6), yielding

$$\mathbf{P}_z^{<}(\mathbf{x},\, \omega_3,\, \theta_0) = \varepsilon_0\int_{-\infty}^{\infty}\frac{\mathrm{d}\omega_1}{2\pi}\chi_{S,zzz}^{(2)}(\omega_3;\, \omega_1,\, \omega_2) \times E_{2z}^{<}(\mathbf{x},\, \omega_1,\, \theta_0)E_{2z}^{*<}(\mathbf{x},\, \omega_2,\, \theta_0), = \mathrm{e}_z P_{0z}^{<}(\omega_3,\, \theta_0)\mathrm{e}^{\mathrm{i}k_x(\omega_3)x}, \quad (A.11)$$

$$\mathbf{P}_x^{<}(\mathbf{x},\, \omega_3,\, \theta_0) = \varepsilon_0\int_{-\infty}^{\infty}\frac{\mathrm{d}\omega_1}{2\pi}\chi_{S,xzx}^{(2)}(\omega_3;\, \omega_1,\, \omega_2) \times E_{2z}^{<}(\mathbf{x},\, \omega_1,\, \theta_0)E_{2x}^{*<}(\mathbf{x},\, \omega_2,\, \theta_0) + \varepsilon_0\int_{-\infty}^{\infty}\frac{\mathrm{d}\omega_1}{2\pi}\chi_{S,xxz}^{(2)}(\omega_3;\, \omega_1,\, \omega_2) \times E_{2x}^{<}(\mathbf{x},\, \omega_1,\, \theta_0)E_{2z}^{*<}(\mathbf{x},\, \omega_2,\, \theta_0), = \mathrm{e}_x P_{0x}^{<}(\omega_3,\, \theta_0)\mathrm{e}^{\mathrm{i}k_x(\omega_3)x}. \quad (A.12)$$

Here $P_{0z}^{<}$ and $P_{0x}^{<}$ are defined respectively as

$$P_{0z}^{<}(\omega_3,\, \theta_0) = \varepsilon_0\sin^2\theta\varepsilon_1^2\int_{-\infty}^{\infty}\frac{\mathrm{d}\omega_1}{2\pi}\chi_{S,zzz}^{(2)} \times (\omega_3;\, \omega_1,\, \omega_2)\frac{A(\omega_1)A^*(\omega_2)}{\varepsilon_2(\omega_1)\varepsilon_2^*(\omega_2)} \times (1 + \tilde{r}_{12}(\omega_1,\, \theta_0))(1 + \tilde{r}_{12}^*(\omega_2,\, \theta_0)), \quad (A.13)$$

$$P_{0x}^{<}(\omega_3,\, \theta_0) = \varepsilon_0\sin\theta_0\cos\theta_0\varepsilon_1\int_{-\infty}^{\infty}\frac{\mathrm{d}\omega_1}{2\pi}\chi_{S,xzx}^{(2)} \times (\omega_3;\, \omega_1,\, \omega_2)\frac{A(\omega_1)A^*(\omega_2)}{\varepsilon_2(\omega_1)} \times (1 + \tilde{r}_{12}(\omega_1,\, \theta_0))(1 - \tilde{r}_{12}^*(\omega_2,\, \theta_0)) + \varepsilon_0\sin\theta_0\cos\theta_0\varepsilon_1\int_{-\infty}^{\infty}\frac{\mathrm{d}\omega_1}{2\pi}\chi_{S,xxz}^{(2)} \times (\omega_3;\, \omega_1,\, \omega_2)\frac{A(\omega_1)A^*(\omega_2)}{\varepsilon_2^*(\omega_2)} \times (1 - \tilde{r}_{12}(\omega_1,\, \theta_0))(1 + \tilde{r}_{12}^*(\omega_2,\, \theta_0)). \quad (A.14)$$

Similarly, the polarization of the upper interface on the metal thin film, $P_{x,z}^{>}$ is given by

$$\mathbf{P}_z^{>}(\mathbf{x},\, \omega_3,\, \theta_0) = \varepsilon_0\int_{-\infty}^{\infty}\frac{\mathrm{d}\omega_1}{2\pi}\chi_{S,xzx}^{(2)}(\omega_3;\, \omega_1,\, \omega_2) \times E_{2z}^{>}(\mathbf{x},\, \omega_1,\, \theta_0)E_{2z}^{*>}(\mathbf{x},\, \omega_2,\, \theta_0), = \mathrm{e}_z P_{0z}^{>}(\omega_3,\, \theta_0)\mathrm{e}^{\mathrm{i}k_x(\omega_3)x}, \quad (A.15)$$

$$\mathbf{P}_x^{>}(\mathbf{x},\, \omega_3,\, \theta_0) = \varepsilon_0\int_{-\infty}^{\infty}\frac{\mathrm{d}\omega_1}{2\pi}\chi_{S,xzx}^{(2)}(\omega_3;\, \omega_1,\, \omega_2) \times E_{2z}^{>}(\mathbf{x},\, \omega_1,\, \theta_0)E_{2x}^{*>}(\mathbf{x},\, \omega_2,\, \theta_0) + \varepsilon_0\int_{-\infty}^{\infty}\frac{\mathrm{d}\omega_1}{2\pi}\chi_{S,xxz}^{(2)}(\omega_3;\, \omega_1,\, \omega_2) \times E_{2x}^{>}(\mathbf{x},\, \omega_1,\, \theta_0)E_{2z}^{*>}(\mathbf{x},\, \omega_2,\, \theta_0), = \mathrm{e}_x P_{0x}^{>}(\omega_3,\, \theta_0)\mathrm{e}^{\mathrm{i}k_x(\omega_3)x}. \quad (A.16)$$

Here $P_{0z}^{>}$ and $P_{0x}^{>}$ are

$$P_{0z}^{>}(\omega_3,\, \theta_0) = \varepsilon_0\sin^2\theta\varepsilon_1\int_{-\infty}^{\infty}\frac{\mathrm{d}\omega_1}{2\pi}\chi_{S,zzz}^{(2)} \times (\omega_3;\, \omega_1,\, \omega_2)\frac{A(\omega_1)A^*(\omega_2)}{\sqrt{\varepsilon_2(\omega_1)}\sqrt{\varepsilon_2^*(\omega_2)}} \times R_z(\omega_1,\, \theta_0)R_z^*(\omega_2,\, \theta_0) \quad (A.17)$$

$$P_{0x}^{>}(\omega_3,\, \theta_0) = \varepsilon_0\sin\theta_0\sqrt{\varepsilon_1}\int_{-\infty}^{\infty}\frac{\mathrm{d}\omega_1}{2\pi}\chi_{S,xzx}^{(2)} \times (\omega_3;\, \omega_1,\, \omega_2)\frac{A(\omega_1)A^*(\omega_2)}{\sqrt{\varepsilon_2(\omega_1)}} \times \left[\frac{\sqrt{\varepsilon_2(\omega_2) - \varepsilon_1\sin^2\theta}}{\sqrt{\varepsilon_2(\omega_2)}}\right]^* R_z(\omega_1,\, \theta_0)R_x^*(\omega_2,\, \theta_0) + \varepsilon_0\sin\theta_0\sqrt{\varepsilon_1}\int_{-\infty}^{\infty}\frac{\mathrm{d}\omega_1}{2\pi}\chi_{S,xxz}^{(2)} \times (\omega_3;\, \omega_1,\, \omega_2)\frac{A(\omega_1)A^*(\omega_2)}{\sqrt{\varepsilon_2^*(\omega_2)}} \times \left[\frac{\sqrt{\varepsilon_2(\omega_1) - \varepsilon_1\sin^2\theta}}{\sqrt{\varepsilon_2(\omega_1)}}\right]R_x(\omega_1,\, \theta_0)R_z^*(\omega_2,\, \theta_0). \quad (A.18)$$

## References


[1] Bloembergen N 1963 Wave propagation in nonlinear electromagnetic media *Proc. IEEE* **51** 124–31

[2] Bloembergen N, Chang R K, Jha S S and Lee C H 1968 Optical second-harmonic generation in reflection from media with inversion symmetry *Phys. Rev.* **174** 813–22

[3] Jha S 1965 Nonlinear optical reflection from a metal surface *Phys. Rev. Lett.* **15** 412–4

[4] Brown F, Parks R E and Sleeper A M 1965 Nonlinear optical reflection from a metallic boundary *Phys. Rev. Lett.* **14** 1029–31

[5] Sonnenberg H and Heffner H 1968 Experimental study of optical second-harmonic generation in silver *J. Opt. Soc. Am.* **58** 209–12

[6] Rudnick J and Stern E A 1971 Second-harmonic radiation from metal surfaces *Phys. Rev.* B **4** 4274–90

[7] Quail J C and Simon H J 1985 Second-harmonic generation from silver and aluminum films in total internal reflection *Phys. Rev.* B **31** 4900–5

[8] Simon H J, Mitchell D E and Watson J G 1974 Optical second-harmonic generation with surface plasmons in silver films *Phys. Rev. Lett.* **33** 1531–4

[9] Chen C K, de Castro A R B and Shen Y R 1981 Surface-enhanced second-harmonic generation *Phys. Rev. Lett.* **46** 145–8

[10] Reinisch R and Neviere M 1983 Electromagnetic theory of diffraction in nonlinear optics and surface-enhanced nonlinear optical effects *Phys. Rev.* B **28** 1870–85

[11] Bouhelier A, Beversluis M, Hartschuh A and Novotny L 2003 Near-field second-harmonic generation induced by local field enhancement *Phys. Rev. Lett.* **90** 013903

[12] Nahata A, Linke R A, Ishi T and Ohashi K 2003 Enhanced nonlinear optical conversion from a periodically nanostructured metal film *Opt. Lett.* **28** 423–5

[13] Palomba S and Novotny L 2008 Nonlinear excitation of surface plasmon polaritons by four-wave mixing *Phys. Rev. Lett.* **101** 056802

[14] Prasad P N 2004 *Nanophotonics* (Hoboken, NJ: Wiley-Interscience)

[15] Novotny L and Hecht B 2006 *Principles of Nano-Optics* (New York: Cambridge University)

[16] Anker J N, Hall W P, Lyandres O, Shah N C, Zhao J and Duyne R P V 2008 Biosensing with plasmonic nanosensors *Nat. Mater.* **7** 442–53

[17] Mayer K M and Hafner J H 2011 Localized surface plasmon resonance sensors *Chem. Rev.* **111** 3828–57

[18] Butet J, Russier-Antoine I, Jonin C, Lascoux N, Benichou E and Brevet P 2012 Sensing with multipolar second harmonic generation from spherical metallic nanoparticles *Nano Lett.* **12** 1697–701

[19] Li Q, Kuo C W, Yang Z, Chen P and Chou K C 2009 Surface-enhanced ir-invisible sum frequency generation vibrational spectroscopy *Phys. Chem. Chem. Phys.* **11** 3436–42

[20] Liz-Marzan L M 2006 Tailoring surface plasmons through the morphology and assembly of metal nanoparticles *Langmuir* **22** 32–41

[21] Ge Y, Cao J, Shen Z, Zheng Y, Chen X and Wan W 2014 Terahertz wave generation by plasmonic-enhanced difference-frequency generation *J. Opt. Soc. Am.* B **31** 1533–8

[22] Lambert A G and Davies P B 2005 Implementing the theory of sum frequency generation vibrational spectroscopy: a tutorial review *Appl. Spectrosc. Rev.* **40** 103–45

[23] Guyot-Sionnest P and Tadjeddine A 1990 Spectroscopic investigations of adsorbates at the metal electrolyte interface using sum frequency generation *Chem. Phys. Lett.* **172** 341–5

[24] Rille A L, Tadjeddine A, Zheng W Q and Peremans A 1997 Vibrational spectroscopy of a au(hkl)-electrolyte interface by *in situ* visible-infrared difference frequency generation *Chem. Phys. Lett.* **271** 95–100

[25] de Barros M R X, Miranda R S, Jedju T M and Becker P C 1995 High-repetition-rate femtosecond mid-infrared pulse generation *Opt. Lett.* **20** 480–2

[26] Emmerichs U, Bakker H J and Kurz H 1994 Generation of high-repetition rate femtosecond pulses tunable in the mid-infrared *Opt. Commun.* **111** 497–501

[27] Lohner A, Kruck P and Ruhle W W 1994 Generation of 200 femtosecond pulses tunable between 2.5 and 5.5 $\mu$m *Appl. Phys.* B **59** 211–3

[28] Kafka J D, Watts M L, Pieterse J W and Herbst R L 1995 Mid-infrared pulse generation using a sub-picosecond opo *Appl. Phys.* B **60** 449–52

[29] Ehret S and Schneider H 1998 Generation of subpicosecond infrared pulses tunable between 5.2 $\mu$m and 18 $\mu$m at a repetition rate of 76 mhz *Appl. Phys.* B **66** 27–30

[30] Fischer C and Sigrist M W 2003 Mid-ir difference frequency generation *Top. Appl. Phys.* **89** 99–143

[31] Kauranen M and Zayats A V 2012 Nonlinear plasmonics *Nat. Photon.* **6** 737–48

[32] Smentkowski V S 2014 *Surface Analysis and Techniques in Biology* (Cham: Springer)

[33] Wang L, Che F, Ponomarenko S A and Chen Z 2013 Plasmon-enhanced spectral changes in surface sum-frequency generation with polychromatic light *Opt. Express* **21** 14159–68

[34] Mandel L and Wolf E 1995 *Optical Coherence and Quantum Optics* (New York: Cambridge University)

[35] Ponomarenko S A, Roychowdhury H and Wolf E 2005 Physical significance of complete spatial coherence of optical fields *Phys. Lett.* A **345** 10–2

[36] Ponomarenko S A and Wolf E 2001 universal structure of field correlations within a fluctuating medium *Phys. Rev.* E **65** 016602

[37] Ponomarenko S A, Agrawal G P and Wolf E 2004 Energy spectrum of a nonstationary ensemble of pulses *Opt. Lett.* **29** 394–6

[38] Yeh P 1988 *Optical Waves in Layered Media, Series in Pure and Applied Optics* (New York: Wiley-Interscience)

[39] Chew W C 1995 *Waves and Fields in Inhomogeneous Media* 2nd edn (New York: Institute of Electrical and Electronics Engineers)

[40] Boyd R W 2003 *Nonlinear Optics* 2nd edn (Boston: Academic)

[41] Mochan W L, Maytorena J A and Mendoza B S 1998 Visible infrared difference frequency generation at cn covered au *Phys. Status Solidi* A **170** 357–63

[42] Evans J M, Spence D E, Burns D and Sibbett W 1993 Dual-wavelength self-mode-locked ti:sapphire laser *Opt. Lett.* **18** 1074–6

[43] Johnson P B and Christy R W 1972 Optical constants of the noble metals *Phys. Rev.* B **6** 4370–9

[44] Maytorena J A, Mendoza B S and Mochan W L 1998 Theory of surface sum frequency generation spectroscopy *Phys. Rev.* B **57** 2569–79